Flow and wall shear stress characterization after endovascular aneurysm repair and endovascular aneurysm sealing in an infrarenal aneurysm model

Johannes T. Boersen, MSc,[a,b,c] Erik Groot Jebbink, MSc,[a,c] Michel Versluis, PhD,[c] Cornelis H. Slump, PhD,[d] David N. Ku, MD, PhD,[e] Jean-Paul P. M. de Vries, MD, PhD,[b] *and* Michel M. P. J. Reijnen, MD, PhD,[a] *Arnhem, Nieuwegein, and Enschede, The Netherlands; and Atlanta, Ga*

ABSTRACT

Background: Endovascular aneurysm repair (EVAR) with a modular endograft has become the preferred treatment for abdominal aortic aneurysms. A novel concept is endovascular aneurysm sealing (EVAS), consisting of dual endoframes surrounded by polymer-filled endobags. This dual-lumen configuration is different from a bifurcation with a tapered trajectory of the flow lumen into the two limbs and may induce unfavorable flow conditions. These include low and oscillatory wall shear stress (WSS), linked to atherosclerosis, and high shear rates that may result in thrombosis. An in vitro study was performed to assess the impact of EVAR and EVAS on flow patterns and WSS.

Methods: Four abdominal aortic aneurysm phantoms were constructed, including three stented models, to study the influence of the flow divider on flow (Endurant [Medtronic, Minneapolis, Minn], AFX [Endologix, Irvine, Calif], and Nellix [Endologix]). Experimental models were tested under physiologic resting conditions, and flow was visualized with laser particle imaging velocimetry, quantified by shear rate, WSS, and oscillatory shear index (OSI) in the suprarenal aorta, renal artery (RA), and common iliac artery.

Results: WSS and OSI were comparable for all models in the suprarenal aorta. The RA flow profile in the EVAR models was comparable to the control, but a region of lower WSS was observed on the caudal wall compared with the control. The EVAS model showed a stronger jet flow with a higher shear rate in some regions compared with the other models. Small regions of low WSS and high OSI were found near the distal end of all stents in the common iliac artery compared with the control. Maximum shear rates in each region of interest were well below the pathologic threshold for acute thrombosis.

Conclusions: The different stent designs do not influence suprarenal flow. Lower WSS is observed in the caudal wall of the RA after EVAR and a higher shear rate after EVAS. All stented models have a small region of low WSS and high OSI near the distal outflow of the stents. (J Vasc Surg 2017;66:1844-53.)

Clinical Relevance: Most endografts for endovascular aortic aneurysm repair involve a modular stent design, and the design could vary in the location of the flow divider. Endovascular aneurysm sealing based on polymer filling of endobags surrounding dual stent frames was recently introduced. This study focuses on effects of a dual-lumen configuration in the abdominal aorta after endovascular aneurysm sealing on flow and wall shear stress proximal and distal to the stents in comparison with two endovascular aneurysm repair endografts and an aneurysm control by in vitro flow visualization.

Endovascular aneurysm repair (EVAR) has become the standard treatment for infrarenal abdominal aortic aneurysms (AAAs). The procedure is related to a lower 30-day mortality rate[1] and shorter rehabilitation period in comparison to open surgical repair. Most endografts involve a modular bifurcated design in which fixation and seal are provided by radial force in the landing zones or proximal fixation with hooks. Stent design varies in the position of the flow divider, the presence of suprarenal fixation, and the attachment of the fabric to the stent frame (exoskeleton or endoskeleton). Endovascular aneurysm sealing (EVAS), whereby the AAA is sealed by polymer-filled endobags surrounding dual 10-mm cobalt-chromium balloon-expandable endoframes, was recently introduced.

The dual-lumen configuration after EVAS is different from an anatomic or EVAR stent bifurcation with a tapered trajectory of the flow lumen into the two limbs.

From the Department of Surgery, Rijnstate Hospital, Arnhem[a]; the Department of Vascular Surgery, St. Antonius Hospital, Nieuwegein[b]; the Department of Physics of Fluids, Faculty of Science and Technology, Technical University of Twente,[c] and MIRA Institute for Biomedical Technology and Technical Medicine, University of Twente,[d] Enschede; and the School of Mechanical Engineering, Georgia Institute of Technology, Atlanta.[e]

Funding for this study was obtained from Endologix Inc and Medtronic.

Author conflict of interest: J.-P.P.M.V. is a consultant for Endologix and Medtronic. M.M.P.J.R. is a consultant for Endologix. D.N.K. is a consultant for Endologix.

Additional material for this article may be found online at www.jvascsurg.org.

Correspondence: Johannes T. Boersen, MSc, Department of Vascular Surgery, St. Antonius Hospital, Koekoekslaan 1, Nieuwegein 3430 EM, The Netherlands (e-mail: j.boersen@antoniusziekenhuis.nl).

The editors and reviewers of this article have no relevant financial relationships to disclose per the JVS policy that requires reviewers to decline review of any manuscript for which they may have a conflict of interest.

0741-5214

http://dx.doi.org/10.1016/j.jvs.2016.10.077

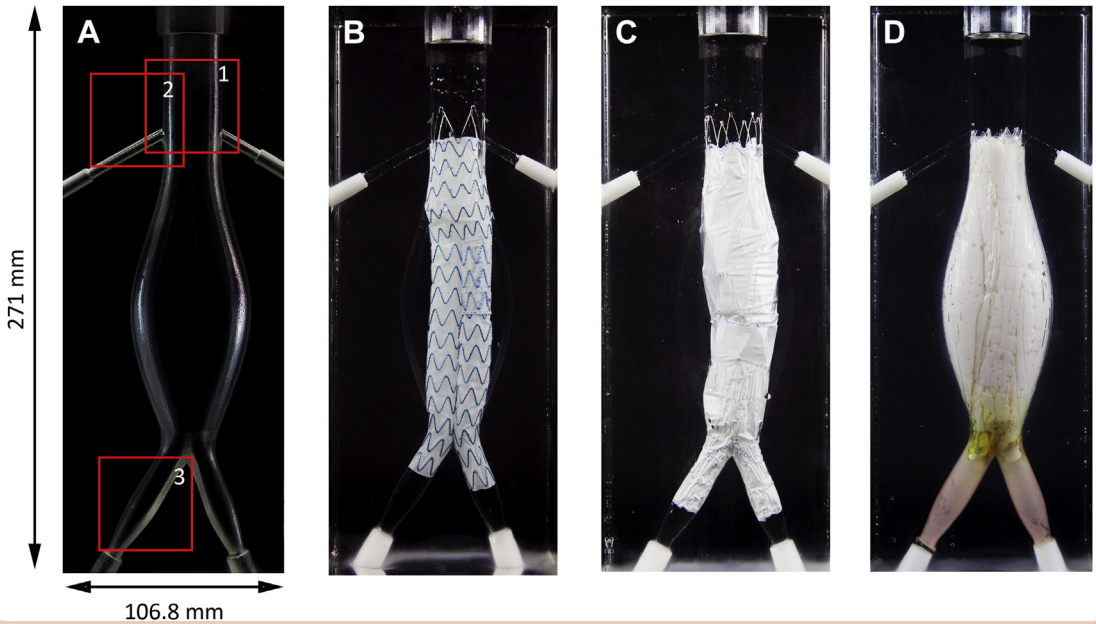

Fig 1. Flow models. **A,** Nonstented, control; indicated are the two-dimensional measurement planes where the flow was captured in the center of the flow lumen. The numbers refer to the three regions of interest: *1*, suprarenal aorta; *2*, right renal artery (RA); and *3*, right common iliac artery (CIA). **B,** Endurant endovascular aneurysm repair (EVAR). **C,** AFX EVAR. **D,** Nellix endovascular aneurysm sealing (EVAS).

This difference in stent design may have different implications regarding flow patterns in the aorta and branch arteries proximal and distal to the stents in comparison with standard modular grafts. A potential mismatch area between the native vessel lumen and the EVAS stents may result in flow recirculation at the transition between the stents and the vessel lumen in the aorta and common iliac arteries (CIAs). Moreover, the transition of the aorta into two 10-mm stents after EVAS may increase vascular resistance, wall shear stress (WSS), and velocity into renal branches.

WSS is defined as the force per unit area acting parallel to the vessel wall due to the local velocity gradient. Low WSS is associated with atherosclerosis[2,3] and subsequent atherothrombotic events,[4,5] and it may occur in regions that present flow recirculation. A low WSS has been defined as <1 Pa for arteries in vivo,[6,7] whereas only extremely low magnitudes (ie, 10^{-2} Pa) have been associated with development of atherosclerosis and blood coagulation.[2,8] Moreover, directional changes in WSS throughout a cardiac cycle (ie, periodic oscillations in WSS) may be found in areas of flow recirculation and have also been associated with development of atherosclerosis.[2,9] A high shear rate (>5000 s^{-1}), referring to the gradient of the local flow velocity near the vessel wall, is associated with acute thrombosis.[10]

The study focuses on effects of a dual-lumen configuration in the abdominal aorta after EVAS on flow and WSS proximal and distal to the stents in comparison with two EVAR endografts and an aneurysm control by in vitro flow visualization.

METHODS

Flow models. Flow phantoms based on an inverse negative mold of a three-dimensional printed AAA model were fabricated (Fig 1, *A*).[11,12] Model geometry was based on a straightforward AAA anatomy with an infrarenal neck diameter of 28 mm, infrarenal neck length of 15 mm, and maximum AAA diameter of 55 mm. A summary of the aortoiliac anatomy of the flow model is provided in Table I. The final design was molded in transparent silicone (Sylgard 184; Dow Corning, Midland, Mich) for optical transparency required for flow visualization. Three different endosystems were implanted: the Endurant II (Medtronic, Minneapolis, Minn), the AFX (Endologix, Irvine, Calif), and the Nellix (Endologix). The flow dividers of the Endurant and AFX are situated 5 cm distal to the most caudal renal artery (RA) and at the native bifurcation, respectively. These models were compared with a control (Fig 1). Stent planning, sizing, and deployment in the models were performed following the standard instructions for use by experienced vascular surgeons (M.M.P.J.R. and J.-P.P.M.V.).

Flow setup. Flow tests were performed under physiologic resting conditions. The setup was based on a two-parameter Windkessel model, including a compliance chamber downstream of the phantom to simulate peripheral vessel impedance.[13] In brief, a pulsatile flow at a rate of 60 beats/min was generated with a physiologic flow rate in a range of 1.6 L/min (peak flow, 3.6 L/min). The inlet section consisted of a 1.2-m tube to ensure a fully developed laminar flow entering the model. At the start

Table I. Phantom geometries

Suprarenal aorta	
Diameter, mm	28
Length, mm	60
Angulation, degrees	0
RAs	
Diameter, mm	6
Length, mm	
Right	54.7
Left	35.1
Angulation, degrees	0
Branching angle, degrees	60
Infrarenal aorta	
Proximal neck diameter, mm	28
Proximal neck length, mm	15
AAA maximum diameter, mm	
AP	40
LR	55
Aortic bifurcation diameter, mm	
AP	28
LR	28
Aneurysm length, mm	115
Infrarenal aorta length, mm	130
Angulation, degrees	0
Iliac arteries	
Diameter, mm	
Upper	14
Middle	14
Lower	8
Length, mm	
Right	86.8
Left	80
Angulation, degrees	0
Takeoff angle, degrees	
Right	30
Left	20

AAA, Abdominal aortic aneurysm; *AP*, anteroposterior; *LR*, left-right; *RAs*, renal arteries.

of each flow experiment, the setup was initiated at a steady flow rate of 1.6 L/min with an equal outflow to renal and iliac branches (0.4 L/min) regulated with needle valves and a mean arterial pressure of 100 mm Hg to equilibrate the system. The relatively larger outflow resistance of the iliac arteries in comparison to the RAs was obtained by a larger diameter of the CIA in comparison to the RA. The fluid level in the compliance vessel was maintained constant throughout the flow experiments with an intended peripheral vessel compliance in a physiologic range around 1.1 mL/mm Hg. This resulted in a reproducible systemic pressure in a range of 120 mm Hg/80 mm Hg.

A blood-mimicking fluid (BMF) was used to obtain a fluid with a viscosity comparable to blood.[14]

Flow visualization. Laser particle imaging velocimetry (PIV) was used to visualize the flow. Fluorescent polymethyl methacrylate particles (rhodamine; size, 1-20 μm; density, 1190 kg/m^3; Dantec Dynamics A/S, Skovlunde, Denmark) were added to the BMF. A pulsed laser (LDY300; Litron, Rugby, England) was used to excite the particles in the BMF and was synchronized with a high-speed camera (FASTCAM SA-5; Photron Inc, West Wycombe, Buckinghamshire, UK) to capture the fluorescent signal. Images were captured at a frame rate of 1000 frames/s. Laser light was focused in a sheet of light to illuminate a thin layer of fluid (<1 mm) within the midplane of the flow lumen. The flow was captured in two dimensions in the anteroposterior (AP) midplane of the flow lumen in three regions of interest: the suprarenal aorta, right RA, and right CIA (Fig 1, *A*). The dimensions of a region of interest were approximately 5 × 5 cm, which were acquired for 10.5 seconds (±10 cardiac cycles) at a frame size of 1024 × 1024 pixels.

Flow analysis. PIV Lab[15] was used to calculate the average displacement of particles in the BMF. The average displacement was determined with a spatial resolution of 0.6 mm by calculating cross-correlations between subsequent frames. Further processing of the data was performed with MATLAB (R2015a; MathWorks, Natick, Mass). In-house built MATLAB scripts were used to calculate the flow direction with an average of 10 cardiac cycles, maximum instantaneous shear rate for each region of interest (s^{-1}), and WSS (Pa). Vector plots of the calculated velocity vectors were made with Tecplot 360 RS (Tecplot, Bellevue, Wash).

WSS was calculated by multiplication of the first-order derivative of the calculated velocity profile near the vessel wall (shear rate; s^{-1}) with the fluid viscosity (μ) $\left(\tau = \frac{\partial y}{\partial x} \times \mu\right)$. The phantom wall was defined by an automated segmentation algorithm in MATLAB, detecting the boundaries of the flow lumen. Subsequently, the algorithm calculated line profiles perpendicular to the vessel wall that cover 50% of the flow lumen length. Natural neighbor interpolation was performed to interpolate the velocity data to a frame size of 1024 × 1024 pixels, and velocity data for each line profile were extracted. Subsequently, the shear rate at the phantom wall was defined on a cubic spline fit of the velocity data based on the best fit determined by the least squares through subsequent velocity points at one velocity vector distance (ie, 16 pixels) and forced zero velocity at the vessel wall (ie, no-slip boundary condition). The laser entered to the right of the model, and WSS calculations were therefore performed for the laser entry side. WSS for each location was calculated by time averaging, referred to as mean WSS in this article, and absolute values were plotted vs

distance, defined by the axial distance on the vessel wall. Oscillations in WSS were assessed by the oscillatory shear index (OSI; Equation 1).[9]

$$OSI = 0.5x\left(1 - \frac{\left|\frac{1}{T}\int_0^T \tau_w dt\right|}{\frac{1}{T}\int_0^T |\tau_w| dt}\right) \quad (1)$$

The OSI ranges from 0 to 0.5, based on the relative period of negative shear vs positive shear through a cardiac cycle per each location. An OSI close to 0.5 indicates severe oscillations in WSS during a cardiac cycle.

Reproducibility of the measurements was analyzed by comparing the flow rate in the suprarenal aorta at the model inlet between the experiments with the different models. Moreover, the average and standard deviation (SD) of WSS and OSI were assessed for the control model without stent to assess time variability of measurements.

RESULTS

The average flow rate at the model inlet in the suprarenal aorta, including all four models, was 1.66 L/min (SD, 0.02 L/min). The average and SD of the flow velocity in the central lumen of the suprarenal aorta in the control are displayed in Fig 2. The average WSS and OSI over 10 cardiac cycles near the wall at this location were 0.063 ± 0.002 Pa (SD, 3.2% of the average WSS) and 0.204 ± 0.001 (SD, 0.6% of the average OSI). The maximum suprarenal aortic wall distention was 0.04 mm (0.1% of the total vessel radius) between peak systolic phase and end-systolic phase and was observed in the EVAS model.

Area 1: Suprarenal aorta. Peak systolic velocity in the center of the suprarenal aorta was comparable for all models with a range of 13.7 to 14.4 cm/s. In all phantoms, including the control, the BMF was accelerated near the renal orifice during the peak systolic phase, and flow reversal was observed near the suprarenal aortic wall during the end-systolic phase (Video 1, online only).

The mean WSS in the suprarenal aorta was similar in all models in a range of 0.05 to 0.95 Pa (Table II). The lowest WSS was found in the proximal part of the suprarenal aorta, comparable in all models around 0.05 to 0.06 Pa (Fig 3, *A*). The OSI was in a similar range for all models (Fig 3, *B*), ranging from a minimum of 0 in all models to a maximum of 0.20 (control) to 0.23 (Endurant; Table II).

The maximum shear rate in the suprarenal aorta varied from 186.9 to 352.9 s^{-1}. The highest shear rate was found in the EVAS model near the RA orifice.

Area 2: RA. The RA flow profile in the EVAR models was comparable to the control (Video 2, online only). A stronger jet flow was observed in the RA in the EVAS model in comparison to EVAR models and control (Video 2, online only; Fig 4). In addition, an increase in flow velocity was found in the center of the distal RA for all stented models.

The mean WSS in the RA varied in a range from 0.1 to 2.3 Pa. WSS was lower on the cranial wall than on the caudal wall for all models, including the control (Table II). All models including the control showed small regions of lower WSS in the RA on the cranial and caudal wall near the RA orifice (Fig 5). In addition, the EVAR models showed a region of low mean WSS on the caudal

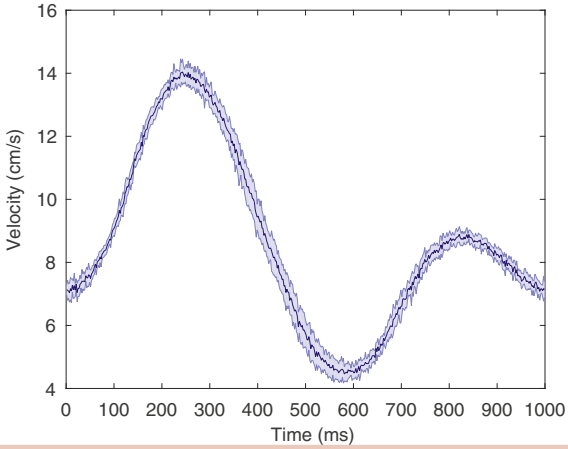

Fig 2. Flow velocity vs time in the center of the suprarenal aorta. The average velocity of 10 cardiac cycles is displayed, and measurement variability is plotted by the standard deviation (SD, shaded error).

Table II. Minimum and maximum of time-averaged wall shear stress (*Pa*) and OSI per vessel segment

	Control	Endurant	AFX	Nellix
Suprarenal				
Right lateral				
WSS (Pa)	0.06-0.48	0.06-0.54	0.05-0.43	0.06-0.95
OSI	0-0.20	0-0.23	0-0.23	0-0.20
Renal artery				
Cranial				
WSS (Pa)	0.66-1.23	0.88-1.35	0.12-1.51	0.44-2.27
OSI	0	0	0	0
Caudal				
WSS (Pa)	0.22-1.43	0.66-1.75	0.57-1.58	0.70-2.30
OSI	0	0	0	0
Common iliac artery				
Medial				
WSS (Pa)	0.11-0.54	0-0.63	0.01-0.80	0-0.67
OSI	0.01-0.11	0.01-0.49	0.01-0.43	0-0.46
Lateral				
WSS (Pa)	0.07-0.61	0-0.70	0-0.79	0.01-0.70
OSI	0.02-0.19	0.01-0.50	0.02-0.49	0-0.48

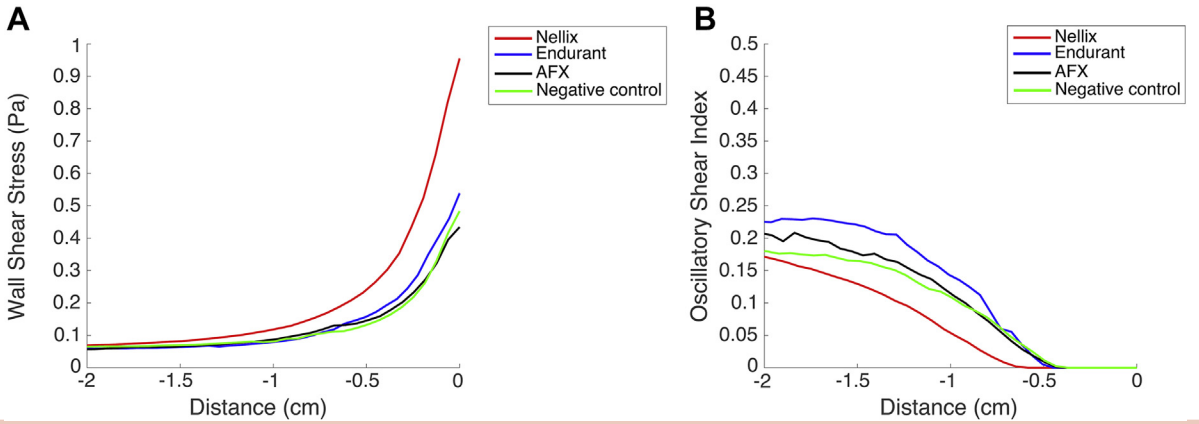

Fig 3. (A) Mean wall shear stress (WSS) and **(B)** oscillatory shear index (OSI) at the right suprarenal aortic wall. Distance is defined as the axial distance along the vessel wall. The cranial renal orifice is located at 0 mm.

wall between 5 and 10 in the AFX and between 5 and 15 mm in the Endurant. The OSI in the RA was near zero for all models including the control.

The maximum shear rate in the RA varied in a range from 325.3 to 717.8 s^{-1}. The highest shear rate was found on the cranial wall in the EVAS model.

Area 3: CIA. A triphasic flow signal was observed in the CIA, with retrograde flow near the vessel wall during the end-systolic phase in all models (Video 3, online only). The stented models showed regions of flow recirculation near the distal end of the stents in the CIA (Fig 6) and low mean WSS in those regions in comparison to the control (Fig 7, *A* and *B*). The regions with low mean WSS ($<10^{-2}$ Pa) were all <10 mm for all stented models. In addition, different flow patterns are seen in the CIA with EVAS. An increase in flow velocity was found at the distal end of the stent in the EVAS model in comparison to the other models (Fig 6, *D*). This region was counterbalanced by a region of retrograde flow on the contralateral wall of the vessel. Similar to the control and EVAR models, the flow in this region returned to a positive direction during the end-diastolic phase. An increase in flow velocity appeared near the distal iliac artery for all models including the negative control (Fig 6), where the model tapers from 14 to 8 mm (Table I). The maximum shear rate in the CIA was comparable for all models, ranging from 324.9 s^{-1} (control medial wall) to 546.5 s^{-1} (AFX lateral wall).

The OSI in the CIA varied in a range from 0 to 0.5. The OSI in the control was at maximum 0.19 (Table II). In the stented models, areas of high OSI (~0.5) were found in regions near the distal end of the stents (Fig 7, *C* and *D*).

DISCUSSION

This study provides a baseline for flow patterns and WSS for various endograft designs. The studied endografts do not substantially affect flow patterns in the lumen center of the suprarenal aorta. Flow velocity and WSS in this area were comparable to the flow in an aneurysm model. The flow was accelerated near the renal ostium, resulting in a higher velocity in the RA in all models. Flow in the RA was forward in direction throughout the entire cardiac cycle, presenting physiologic flow conditions.[8] The acceleration of flow near the renal ostium was larger for EVAS, resulting in a stronger jet flow and higher shear rate in the RA in comparison to the other models, most likely because of transition of the suprarenal aortic flow into the two 10-mm endoframes. Low-flow velocity was found in the proximal RA of the EVAR models near the caudal wall, presenting an area of lower WSS in comparison to the control. In addition, recirculating flow was observed near the distal end of the stent in all stented models, presenting regions of low mean WSS ($<10^{-2}$ Pa) and high OSI (~0.5) in comparison to the control.

Low mean WSS and severe oscillations in WSS have been associated with atherosclerosis[2,3] by initiating endothelial responses that result in intimal thickening of the vessel wall. In this study, the mean WSS in the suprarenal aorta was in a range similar to that reported by Moore,[2] and this was fairly low considering values that have been reported for arterial baseline WSS (1-7 Pa).[6,7] The regions with low WSS on the suprarenal aortic wall were comparable in axial distance along the wall between the different models including the control. The values found for mean WSS in the RA were mostly in accordance with the control, but a region of lower mean WSS (<1 Pa) was observed in the caudal wall of the proximal RA in both EVAR models. This lower WSS may enhance development of atherosclerosis in those areas. Renal stenosis after EVAR has been scarcely documented and could also be related to a suprarenal stent wire traversing the renal ostium or partial coverage of the renal ostium by graft material. The potential additional effects of this area of lower WSS in the caudal wall of the RA remain to be investigated. EVAR has been associated with a higher risk of decline in renal

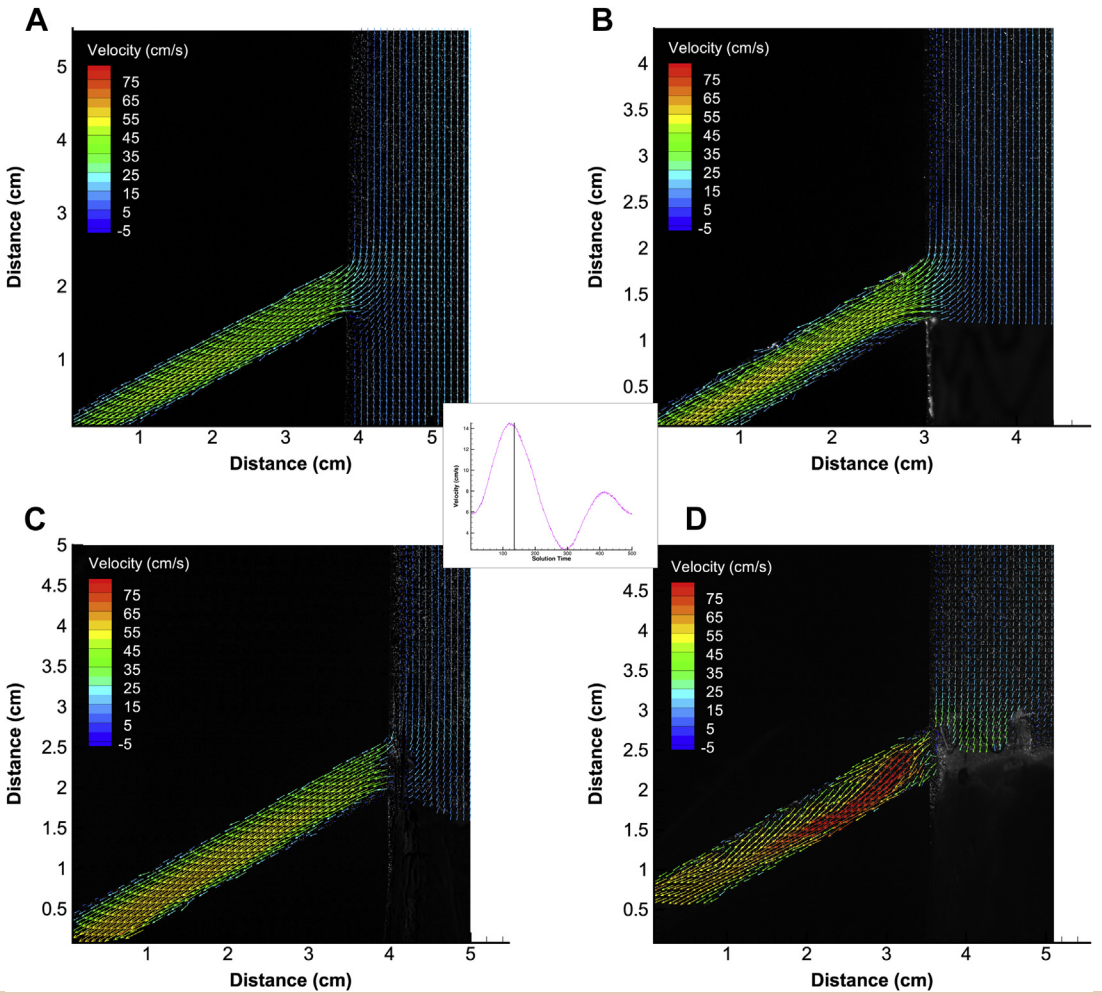

Fig 4. Peak systolic phase velocities in the right renal artery (RA). **A,** Control. **B,** Endurant. **C,** AFX. **D,** Nellix. Low-velocity regions were observed at the inflow section near the caudal wall of the RA for all stented models, which were more apparent for the endovascular aneurysm repair (EVAR) models **(B** and **C),** and the flow velocity was enhanced at the renal inflow section of the Nellix model **(D)**.

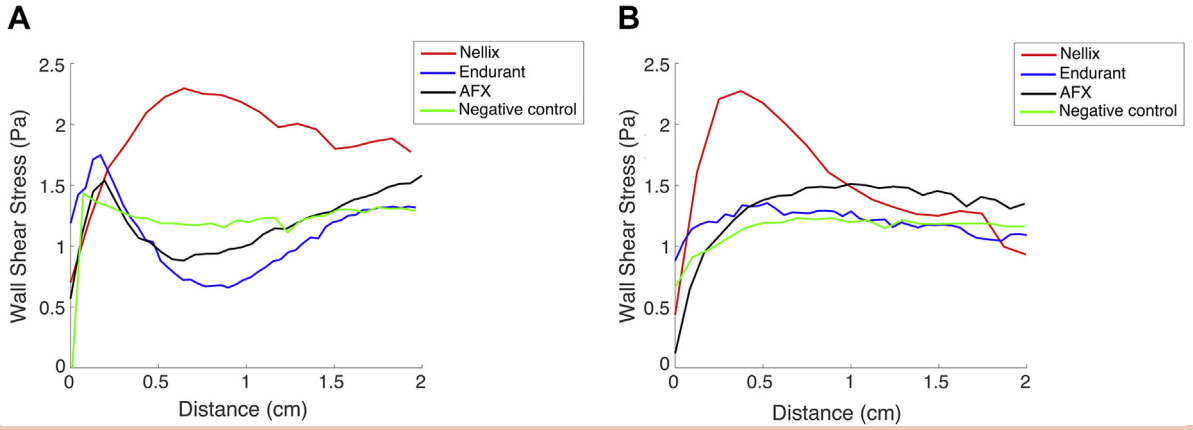

Fig 5. Time-averaged wall shear stress (WSS) at the right renal artery (RA). **A,** Caudal. **B,** Cranial wall of RA. The scale is given as the axial distance from the renal orifice at 0 mm.

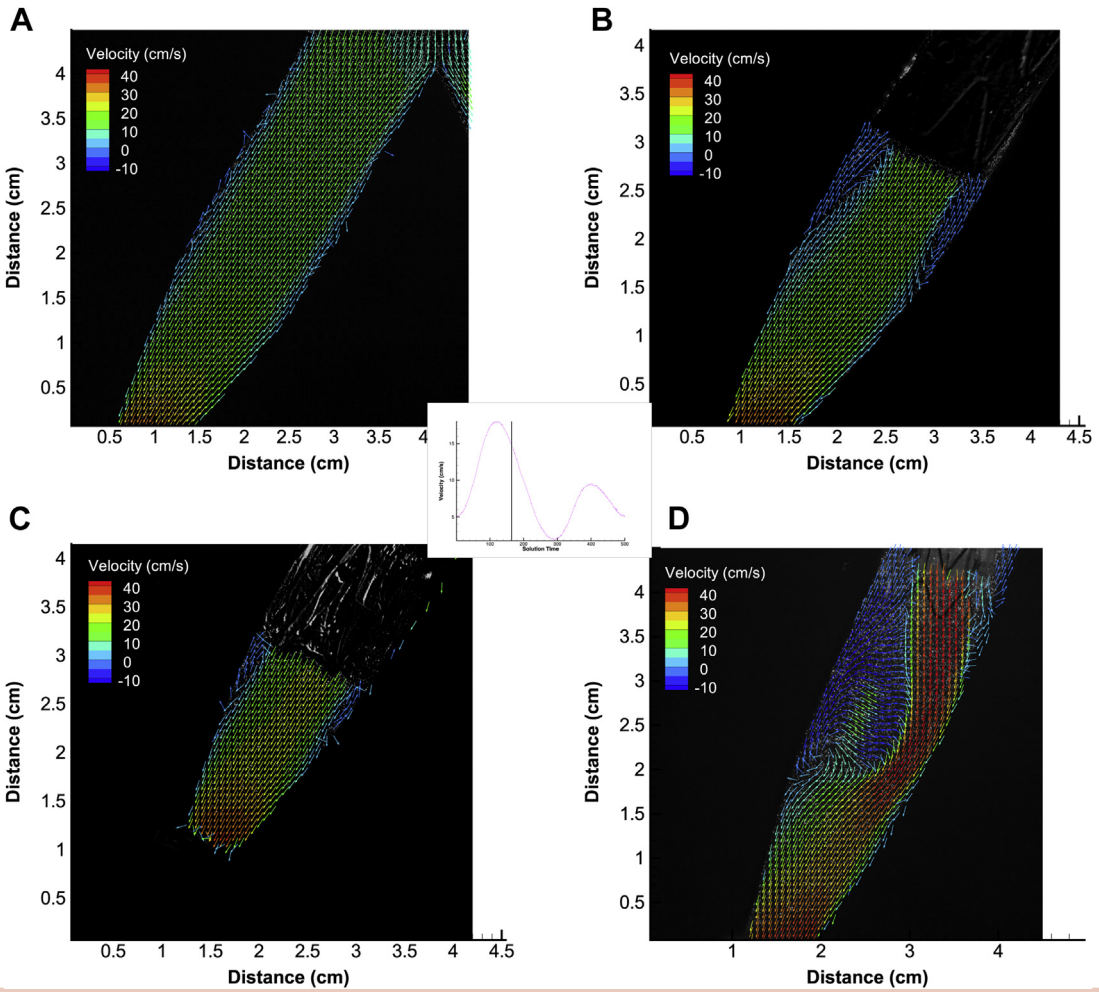

Fig 6. Velocity during peak systolic phase in the right common iliac artery (CIA). **A,** Control. **B,** Endurant. **C,** AFX. **D,** Nellix. Recirculating flow was observed near the distal end of the stent in all models. The velocity accelerates toward the distal artery in all models, where the limb tapers from 14 to 8 mm.

function in comparison to open surgical repair mostly during the first postprocedural year.[16] Remodeling and adaptation of the vessel to flow alterations after EVAR are assumed to occur during a longer time. Moreover, age (>75 years), thromboembolic complications, and use of nephrotoxic contrast material have been associated with a decline in renal function after EVAR,[17,18] and these factors may explain the poorer outcome of long-term renal function after endovascular repair in comparison to open surgical repair.

In the EVAS model, regions of higher velocity and WSS were observed in the RA. The transition of the aorta into the two 10-mm endoframes that are surrounded by the upper margin of the polymer-filled endobags may contribute to the observed increase in peak velocity in the RA. In addition, the vascular stiffness is likely to increase compared with the EVAR model. In general, it is advised to position the endobags immediately below the RAs, such that the proximal 4-mm bare stents are at the level of the orifice of one or both RAs. The endoframes were positioned with the proximal end of the stent at the proximal edge of the RA, and the renal flow profile may be influenced by the covered proximal part of the stent (4 mm from the proximal bare stent), concerning a renal orifice diameter of 6 mm, as the renal ostium was not partially obstructed by the endobag (Fig 4, *D*). Segalova et al performed computational fluid dynamics with the proximal bare stent partially in the segment of the renal orifice after EVAS, suggesting minimal effect of the proximal stent struts on renal flow, whereas the flow velocity and WSS (and shear rate) in the RA were comparable to baseline. An increase in WSS was found only close to the stent struts.[19] An intended lower positioning of the EVAS stents in this study may have improved the renal flow profile, and this will be the subject of a future study. That position, however, could reduce the sealing zone and thus increase the risk of other problems, including migration and type IA endoleak. Maximum shear rates were well below the pathologic threshold (maximum of 717.8 s^{-1}

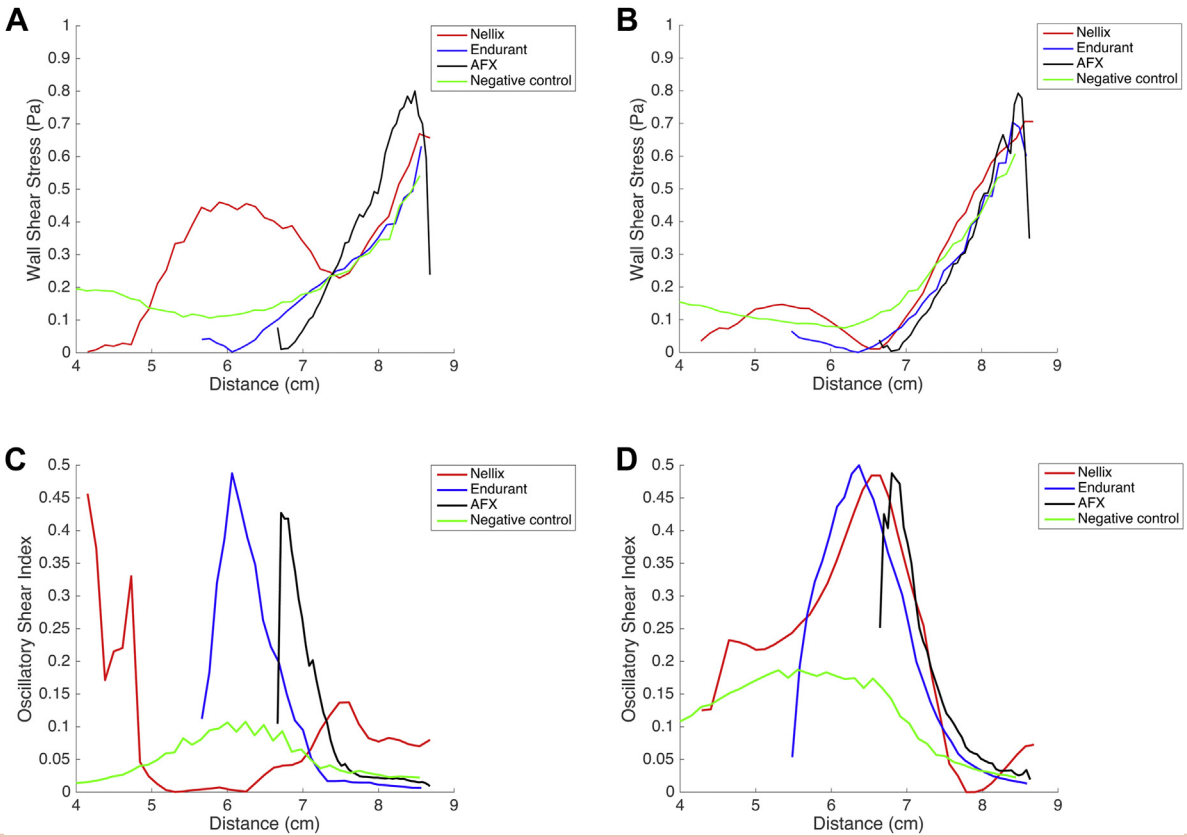

Fig 7. Time-averaged wall shear stress (WSS) and oscillatory shear index (OSI) at the right common iliac artery (CIA). **A,** WSS at the medial wall. **B,** WSS at the right lateral wall. **C,** OSI at the medial wall. **D,** OSI at the right lateral wall of the vessel. The start of each curve refers to the distal end of the stent or bifurcation (control), whereas the end of each curve refers to the distal connection of the model in the CIA.

vs >5000 s^{-1}),[10] suggesting that acute events, such as acute thrombosis, are unlikely to be caused by the observed flow alterations after EVAS.

Regions with high OSI (~0.5) were observed in the CIA of both EVAR and EVAS models. Flow recirculation in the CIA near the distal end of the stents was most likely caused by the transition between the stent and phantom vessel wall. In addition, the EVAS model showed an increase in flow velocity near the CIA at the distal stent in comparison to the other models. Increased velocity observed in this study was mainly due to a pressure drop resulting from transition of the 10-mm stent frame into a 14-mm vessel. This phenomenon may add to a larger area of recirculation and retrograde flow near the lateral wall. Flow recirculation for seconds has been associated with thrombosis.[20] All flow returned to a forward direction during the end-diastolic phase, and there were no areas with stagnant flow, and therefore it is not likely that the risk of limb thrombosis will be increased after EVAS. So far, no substantial differences have been observed regarding stent graft occlusion for EVAR and EVAS devices. Limited data on post-EVAS follow-up exist. The incidence of limb occlusions after 1 year has been reported around 4% and 5% for EVAR[21] and EVAS,[22] respectively. Short and intermediate patency of stent grafts may be more dependent on flow alterations in the endograft. Endograft kinking and subsequent stenosis have been found to be risk factors for loss of both short- and intermediate-term graft patency.[23,24]

Limitations. A limitation of this study is that flow analysis was limited to a two-dimensional plane in the center of the flow lumen, with potential bias due to out-of-plane motion of the tracer particles. As a result, secondary flow, including recirculation of tracer particles, could not be captured accurately. Moreover, flow visualization was limited to the AP midplane, and differences in flow may be found in another direction (ie, lateral midplane).

A straightforward anatomy was used to examine the influence of the stent graft only on flow in the regions of interest. The model geometry could be of influence on the measured flow profile, and these effects may be different for the studied endografts. Inclusion of aortoiliac angulation results in lower velocity near the inner curve with potential plaque formation.[5] However, inclusion of angulation in the AP plane makes

measurements a true challenge with the current technique. In addition, higher location of one of the branch orifices may result in a larger recirculation zone with lower WSS near the suprarenal aortic wall. Moreover, other in vitro studies demonstrated a higher WSS (and shear rate) at a higher heart rate,[25] whereas flow experiments in this study were performed only under physiologic resting conditions.

The variation in flow rate between the experiments including all models was low (mean, 1.66 L/min; SD, 0.02 L/min), suggesting that the experiments were reproducible. The slight variations in flow rate may be caused by the different stents in the models. In addition, the slight variations in flow rate may add to slight variations in WSS and OSI between the models in the studied regions of interest.

Flow in the endograft could not be assessed in this study as the graft material did not allow optical access, and as a result, flow near the bifurcation could not be assessed for the EVAR models. Transparent stent grafts[12] can be used to analyze the flow in these areas with laser PIV. Ultrasound PIV could overcome this problem. In addition, laser PIV of multiple planes in two dimensions in the flow lumen (eg, stereo PIV) or computational fluid dynamics validated with the results of this study can aid in an accurate flow characterization in those areas. The end-systolic phase and peak diastolic phase appeared delayed by 84 ms and 60 ms, resulting in a slightly higher volumetric flow per cycle, and time-averaged WSS may be slightly overestimated.

The model compliance was not measured, but only minimal suprarenal aortic wall distention was determined during the cardiac cycle (maximum of 0.1% of the total vessel radius). The use of a stiff model may be justified because of stiffening of the vasculature in atherosclerosis and the elderly[26]; however, the results of this study cannot be generalized for all AAA patients. The use of a more compliant model will usually result in lower WSS and lower shear rates.[27] This study demonstrated no significant difference in flow between the different models in the studied regions of interest, and a more elastic wall will only result in changes in absolute values. The effects of a more elastic wall on flow (ie, a lower WSS) will be mainly dependent on variations in local wall characteristics between patients.

The glycerol in the BMF is newtonian, and WSS values may therefore be overestimated. Nevertheless, blood flow in large vessels is supposed to be newtonian.[8] The concentration of tracer particles in the BMF was small (0.021% of total volume), and it is therefore not likely that these will influence the viscosity of the BMF and WSS calculations. However, the no-slip (boundary) condition may not be accurate for tracer particles near the model wall.

CONCLUSIONS

The location of the flow divider does not influence suprarenal flow. Low WSS is observed in the caudal wall of the RA after EVAR and an increased shear rate after EVAS, whereas all stented models have a small area of low WSS and high OSI near the distal outflow of the stents.

We would like to thank H. Kuipers (Department of Robotics and Mechatronics, University of Twente) for assistance in the design and construction of the flow model setup and C. Sun and M. Varghese (Department of Physics and Fluids, University of Twente) for advice on the laser particle imaging velocimetry technique.

AUTHOR CONTRIBUTIONS

Conception and design: JB, EGJ, JV, MR
Analysis and interpretation: JB, EGJ, MV, CS, DK, JV, MR
Data collection: JB, EGJ
Writing the article: JB, JV, MR
Critical revision of the article: EGJ, MV, CS, DK, JV, MR
Final approval of the article: JB, EGJ, MV, CS, DK, JV, MR
Statistical analysis: Not applicable
Obtained funding: EGJ, MR
Overall responsibility: MR

REFERENCES

1. Stather P, Sidloff D, Dattani N, Choke E, Bown M, Sayers R. Systematic review and meta-analysis of the early and late outcomes of open and endovascular repair of abdominal aortic aneurysm. Br J Surg 2013;100:863-72.
2. Moore JE, Xu C, Glagov S, Zarins CK, Ku DN. Fluid wall shear stress measurements in a model of the human abdominal aorta: oscillatory behavior and relationship to atherosclerosis. Atherosclerosis 1994;110:225-40.
3. Pedersen EM, Agerbaek M, Kristensen IB, Yoganathan AP. Wall shear stress and early atherosclerotic lesions in the abdominal aorta in young adults. Eur J Vasc Endovasc Surg 1997;13:443-51.
4. Cheng C, Tempel D, van Haperen R, van der Baan A, Grosveld F, Daemen MJ, et al. Atherosclerotic lesion size and vulnerability are determined by patterns of fluid shear stress. Circulation 2006;113:2744-53.
5. Slager C, Wentzel J, Gijsen F, Schuurbiers J, van der Wal A, van der Steen A, et al. The role of shear stress in the generation of rupture-prone vulnerable plaques. Nat Clin Pract Cardiovasc Med 2005;2:401-7.
6. Malek AM, Alper SL, Izumo S. Hemodynamic shear stress and its role in atherosclerosis. JAMA 1999;282:2035-42.
7. Hathcock JJ. Flow effects on coagulation and thrombosis. Arterioscler Thromb Vasc Biol 2006;26:1729-37.
8. Ku DN, Giddens DP, Zarins CK, Glagov S. Pulsatile flow and atherosclerosis in the human carotid bifurcation. Positive correlation between plaque location and low oscillating shear stress. Arteriosclerosis 1985;5:293-302.
9. He X, Ku DN. Pulsatile flow in the human left coronary artery bifurcation: average conditions. J Biomech Eng 1996;118:74-82.
10. Casa LD, Deaton DH, Ku DN. Role of high shear rate in thrombosis. J Vasc Surg 2015;61:1068-80.

11. Geoghegan P, Buchmann N, Spence C, Moore S, Jermy M. Fabrication of rigid and flexible refractive-index-matched flow phantoms for flow visualisation and optical flow measurements. Exp Fluids 2012;52:1331-47.
12. Groot Jebbink E, Grimme FA, Goverde PC, van Oostayen JA, Slump CH, Reijnen MM. Geometrical consequences of kissing stents and the Covered Endovascular Reconstruction of the Aortic Bifurcation configuration in an in vitro model for endovascular reconstruction of aortic bifurcation. J Vasc Surg 2015;61:1306-11.
13. Groot Jebbink E, Mathai V, Boersen JT, Sun C, Slump CH, Goverde PC, et al. Hemodynamic comparison of stent configurations used for aortoiliac occlusive disease [published online ahead of print October 12, 2016]. J Vasc Surg doi: 10.1016/j.jvs.2016.07.128.
14. Yousif MY, Holdsworth DW, Poepping TL. A blood-mimicking fluid for particle image velocimetry with silicone vascular models. Exp Fluids 2011;50:769-74.
15. Thielicke W, Stamhuis EJ. PIVlab—towards user-friendly, affordable and accurate digital particle image velocimetry in MATLAB. JORS 2014;2:e30.
16. Saratzis A, Bath MF, Harrison S, Sayers RD, Mahmood A, Sarafidis P, et al. Long-term renal function after endovascular aneurysm repair. Clin J Am Soc Nephrol 2015;10:1930-6.
17. Walsh SR, Tang TY, Boyle JR. Renal consequences of endovascular abdominal aortic aneurysm repair. J Endovasc Ther 2008;15:73-82.
18. Mills JL, Duong ST, Leon LR, Goshima KR, Ihnat DM, Wendel CS, et al. Comparison of the effects of open and endovascular aortic aneurysm repair on long-term renal function using chronic kidney disease staging based on glomerular filtration rate. J Vasc Surg 2008;47:1141-9.
19. Segalova PA, Rao KV, Zarins CK, Taylor CA. Computational modeling of shear-based hemolysis caused by renal obstruction. J Biomech Eng 2012;134:021003.
20. Basciano C, Kleinstreuer C, Hyun S, Finol E. A relation between near-wall particle-hemodynamics and onset of thrombus formation in abdominal aortic aneurysms. Ann Biomed Eng 2011;39:2010-26.
21. van Zeggeren L, Gonçalves FB, van Herwaarden JA, Zandvoort HJ, Werson DA, Vos J, et al. Incidence and treatment results of Endurant endograft occlusion. J Vasc Surg 2013;57:1246-54.
22. Böckler D, Holden A, Thompson M, Hayes P, Krievins D, de Vries JP, et al. Multicenter Nellix EndoVascular Aneurysm Sealing system experience in aneurysm sac sealing. J Vasc Surg 2015;62:290-8.
23. Cochennec F, Becquemin JP, Desgranges P, Allaire E, Kobeiter H, Roudot-Thoraval F. Limb graft occlusion following EVAR: clinical pattern, outcomes and predictive factors of occurrence. Eur J Vasc Endovasc Surg 2007;34:59-65.
24. Fransen GA, Desgranges P, Laheij RJ, Harris PL, Becquemin J. Frequency, predictive factors, and consequences of stent-graft kink following endovascular AAA repair. J Endovasc Ther 2003;10:913-8.
25. Taylor CA, Cheng CP, Espinosa LA, Tang BT, Parker D, Herfkens RJ. In vivo quantification of blood flow and wall shear stress in the human abdominal aorta during lower limb exercise. Ann Biomed Eng 2002;30:402-8.
26. O'Rourke MF, Hashimoto J. Mechanical factors in arterial aging: a clinical perspective. J Am Coll Cardiol 2007;50:1-13.
27. Perktold K, Rappitsch G. Computer simulation of local blood flow and vessel mechanics in a compliant carotid artery bifurcation model. J Biomech 1995;28:845-56.

Submitted Jul 6, 2016; accepted Oct 10, 2016.

Additional material for this article may be found online at www.jvascsurg.org.